Science Advances

AAAS

advances.sciencemag.org/cgi/content/full/3/6/e1602263/DC1

Supplementary Materials for

Reconstructed storm tracks reveal three centuries of changing moisture delivery to North America

Erika K. Wise and Matthew P. Dannenberg

Published 7 June 2017, *Sci. Adv.* **3**, e1602263 (2017)
DOI: 10.1126/sciadv.1602263

This PDF file includes:

Supplementary Materials

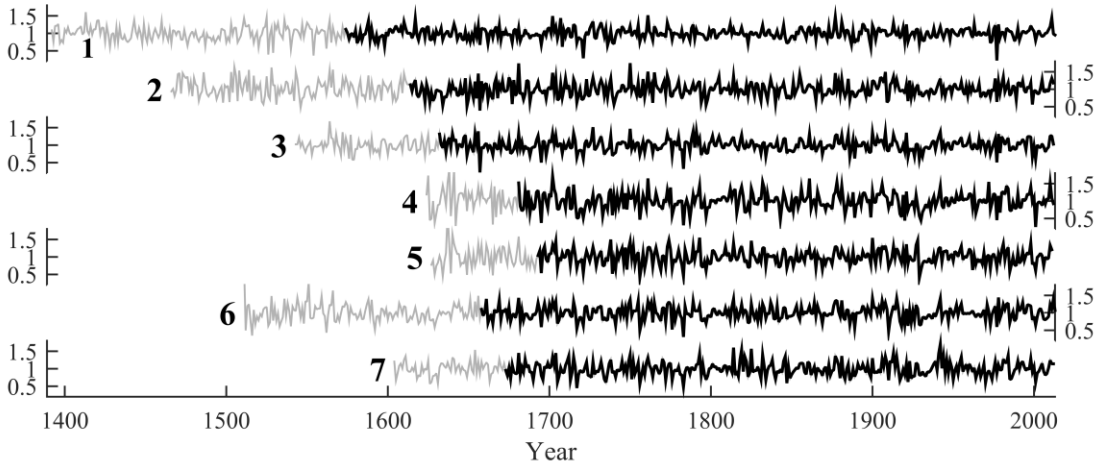

fig. S1. Tree-ring chronologies for seven sites in the U.S. PNW. Ring widths for each tree were detrended using a cubic spline two-thirds the length of each individual series and combined to form site chronologies. The full chronology is shown in gray; the portion of each series with subsample signal strength (SSS) (*26*) greater than 0.85 is shown in black. All seven series reached SSS>0.85 by 1693 CE. Chronology labels 1-7 correspond to site locations shown in Fig. 1A. Chronology mean sensitivities ranged from 0.26 to 0.33 and series intercorrelation from 0.59 to 0.71.

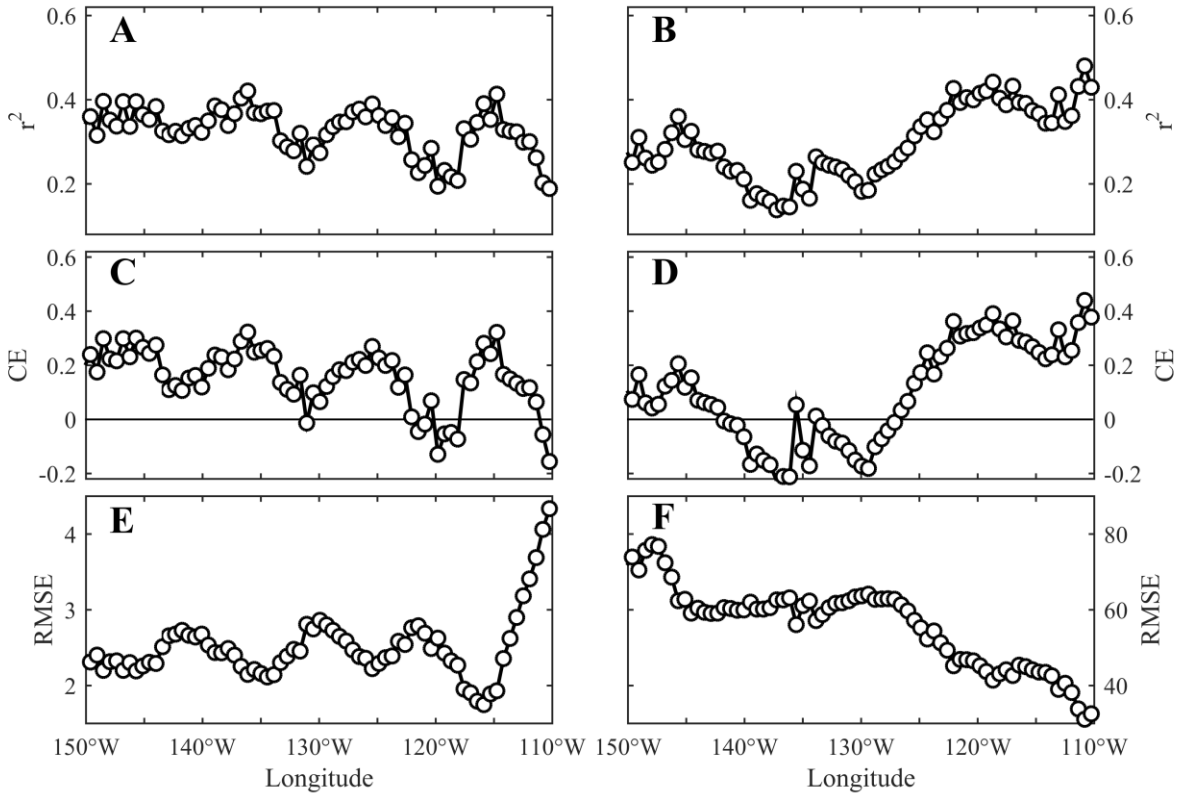

fig. S2. Validation statistics for the storm-track reconstruction at each longitude. The skill of the reconstruction models for each longitude was assessed using a leave-one-out cross-validation procedure and was measured by: (**A**) the coefficient of determination (r^2) between the instrumental storm track position and composite-plus-scale (CPS)-predicted (*28*) storm track position; (**B**) r^2 between the instrumental storm track intensity and CPS-predicted storm track intensity; (**C**) the Coefficient of Efficiency between the instrumental storm track position and the CPS-predicted storm track position (where Coefficient of Efficiency values > 0 indicate predictive skill); (**D**) the Coefficient of Efficiency between the instrumental storm track intensity and the CPS-predicted storm track intensity; (**E**) Root Mean Square Error (RMSE) between the instrumental storm track position and the CPS-predicted storm track position; and (**F**) RMSE between the instrumental storm track intensity and the CPS-predicted storm track intensity.

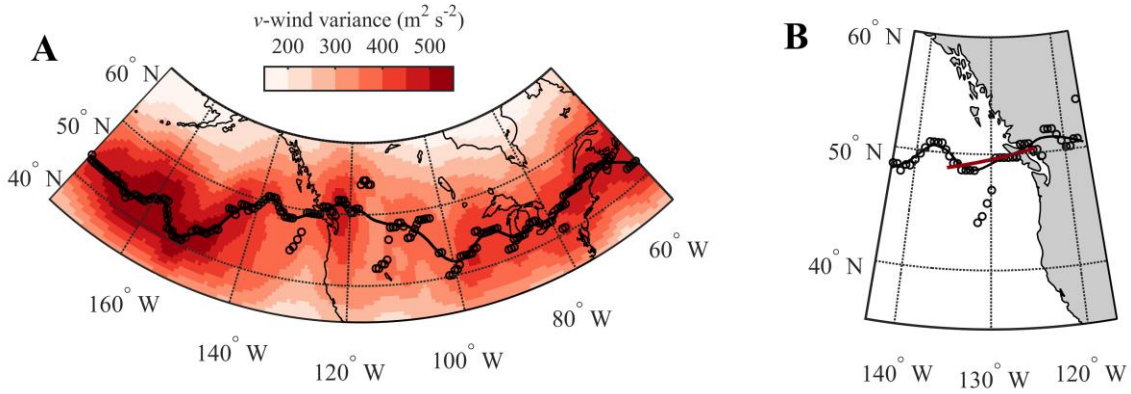

fig. S3. Delineation of the storm track in an example year (1988). (**A**) The storm track was estimated as the latitude of maximum *v*-wind variance (circles) and smoothed with a robust loess filter (black line) to reduce noise. (**B**) Storm track position was determined by fitting a straight line (using ordinary least squares regression) to the smoothed storm track latitude over the region 136°W to 124°W. Storm track position was defined as the latitude where the fitted line crossed 124°W.

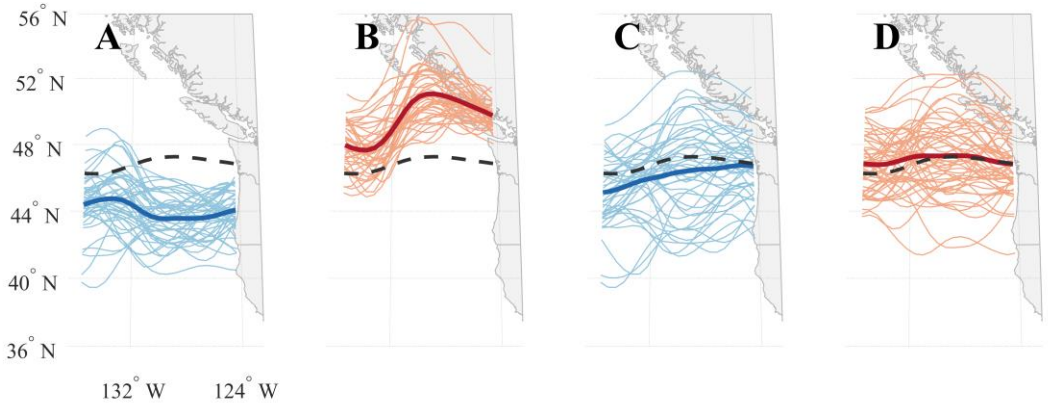

fig. S4. Extremes in latitude and intensity in reconstructed storm tracks over the reconstruction period of 1693 to 1995 CE. Reconstructed storm tracks (smoothed with a robust loess filter) in years that were one standard deviation below the mean (**A** and **C**) and one standard deviation above the mean (**B** and **D**) over the reconstructed record based on position (A and B) and intensity (C and D). Mean storm track for all years shown with dotted black line; mean storm track for each subset shown with dark blue and red lines.

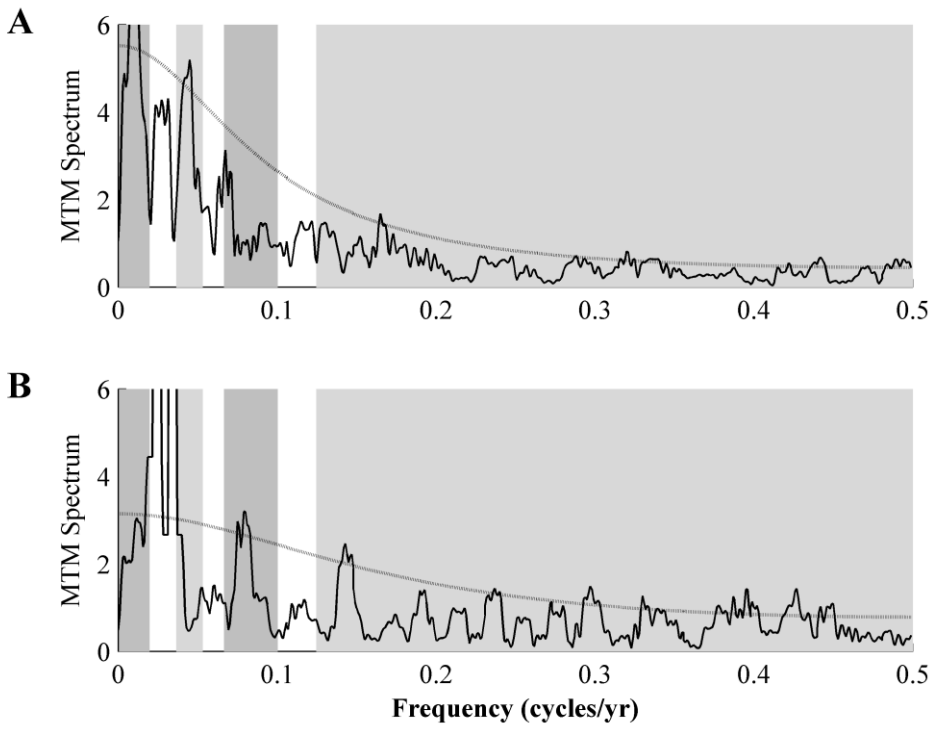

fig. S5. Spectral power in the storm-track reconstructions. MTM spectral analysis of normalized reconstructed storm-track position (**A**), and intensity (**B**) over the 1693-1995 CE time period, tested against a red noise null hypothesis and reshaped to remove harmonic signals. Dotted lines denote the 90% significance level. Gray highlighting emphasizes important frequency bands (left to right in each subplot): pentadecadal or longer (>50 years), bidecadal (19-27 year), decadal (10-15 year), and ENSO (2-8 year). MTM analyses were performed using the SSA-MTM Toolkit (*29*) available at http://research.atmos.ucla.edu/tcd//ssa/.

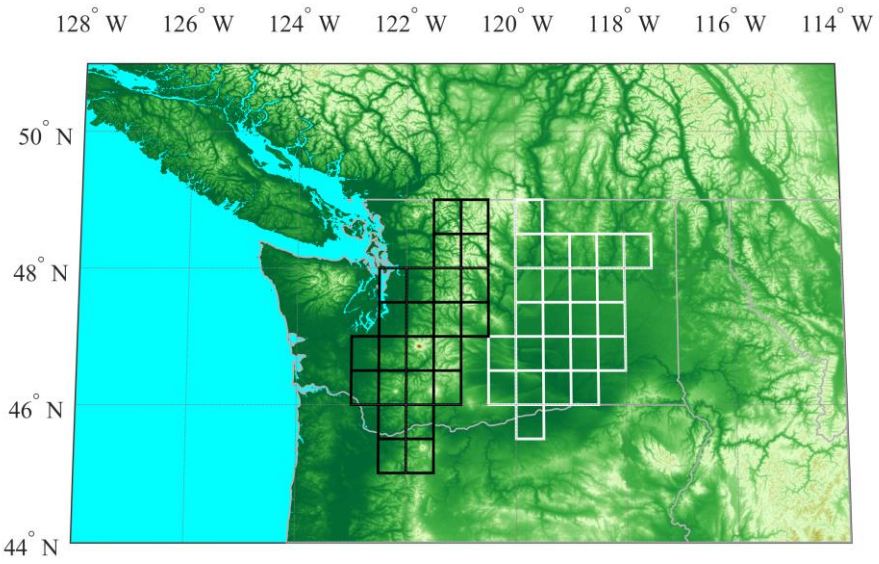

fig. S6. Grid cells representing windward and leeward regions across the Cascade Range. Windward (black grid cells) and leeward (white grid cells) were separated for analyses examining SPI patterns across the region. The selected grid cells were those that were considered robust in the SPI reconstruction (*37*) (Coefficient of Efficiency > 0) and that represent regions with differing responses during El Niño years as shown in Fig. 1A. Shaded background displays topography of the region.

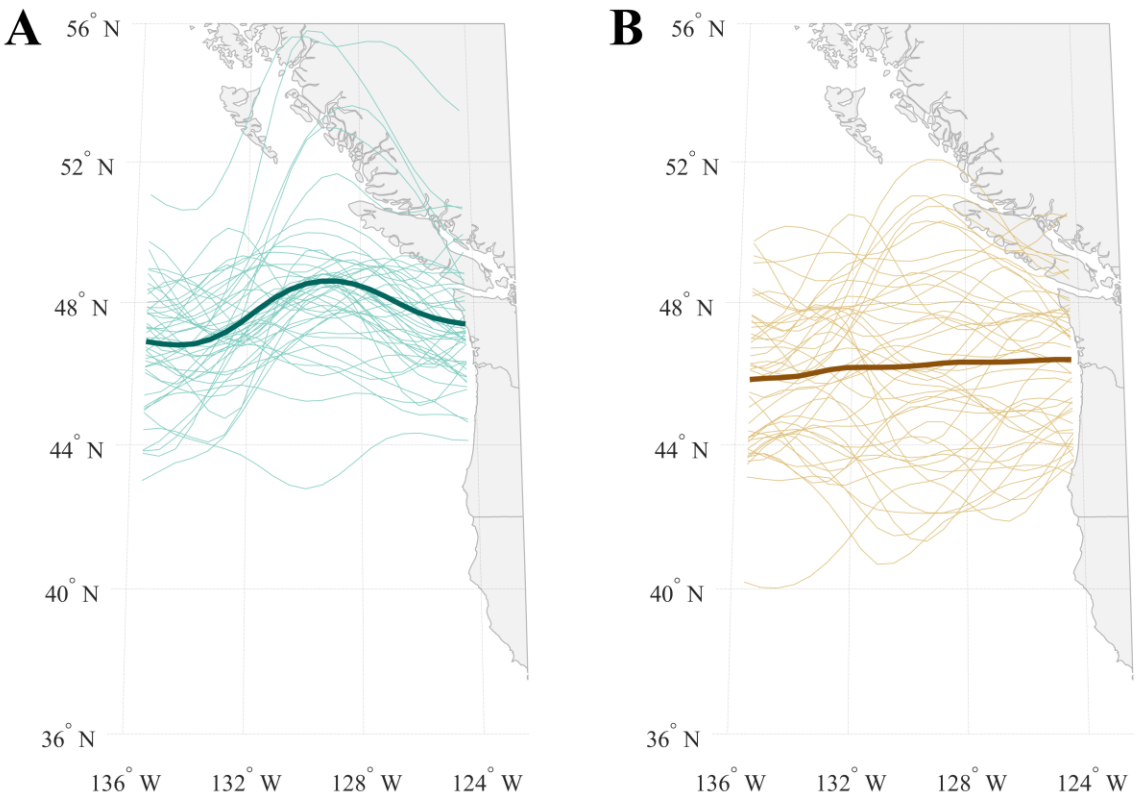

fig. S7. Storm track in La Niña and El Niño years based on an alternative ENSO reconstruction from 1693 to 1995 CE. Composites of yearly storm tracks smoothed with a robust loess filter during La Niña (**A**) and El Niño (**B**) years, determined using a Jul-Jun NINO3.4 SST reconstruction developed by merging existing ENSO proxy reconstructions into one that captures and highlights their common ENSO signal (*45*). Here, we have characterized years in this reconstruction as El Niño or La Niña based on +/- one standard deviation from mean conditions.

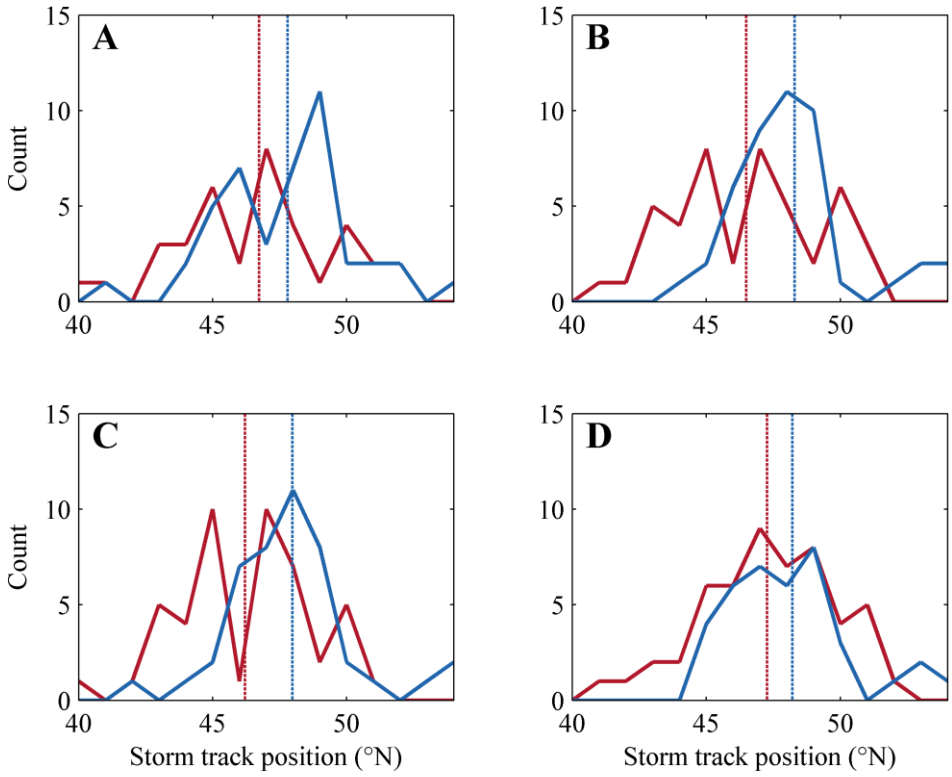

fig. S8. Distribution of reconstructed storm-track position in La Niña and El Niño years. Distribution of reconstructed storm-track latitude at 124°W longitude in La Niña (blue) and El Niño (red) years based on four different ENSO reconstructions: (**A**) 1728-1995 CE (*44*); (**B**) 1693-1977 CE (*45*); (**C**) 1693-1995 CE [(*62*), https://www.ncdc.noaa.gov/paleo/study/8704]; and (**D**) 1693-1980 CE [(*63*), http://www.cricyt.edu.ar/paleo/ei/ei_data/ninocold-recon.dat]. Dotted blue and red vertical lines indicate the mean storm track position in La Niña and El Niño years, respectively. See table S2 for additional information on these reconstructions.

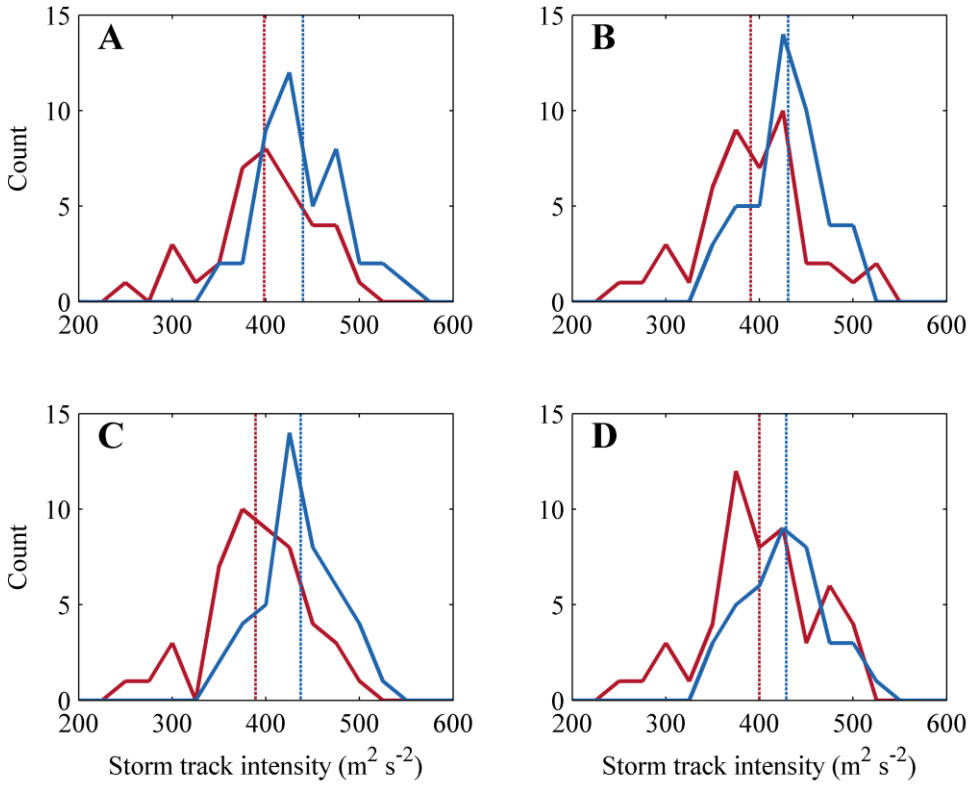

fig. S9. Distribution of reconstructed storm-track intensity in La Niña and El Niño years. Distribution of reconstructed storm-track intensity at 124°W longitude in La Niña (blue) and El Niño (red) years based on four different ENSO reconstructions: (**A**) 1728-1995 CE (*44*); (**B**) 1693-1977 CE (*45*); (**C**) 1693-1995 CE [(*62*), https://www.ncdc.noaa.gov/paleo/study/8704]; and (**D**) 1693-1980 CE [(*63*), http://www.cricyt.edu.ar/paleo/ei/ei_data/ninocold-recon.dat]. Dotted blue and red vertical lines indicate the mean storm track position in La Niña and El Niño years, respectively. See table S2 for additional information on these reconstructions.

table S1. Reconstructed storm-track latitude and intensity in years with anomalous precipitation patterns.

	SPI subset	Latitude (°N)*	Intensity (m^2 s^{-2})*
Mean (Std Dev)	BD	48.1 (2.9)	412.2 (46.9)
	LDWW	48.2 (2.3)	446.9 (41.9)
	LWWD	46.8 (1.6)	376.5 (45.1)
	BW	48.8 (1.5)	430.2 (60.5)
Significance^	All Groups	$p \leq 0.1$	$p \leq 0.01$
	LWWD-LDWW	$p \leq 0.05$	$p \leq 0.01$
	LWWD-BD	$p \leq 0.1$	$p \leq 0.05$
	LWWD-BW	$p \leq 0.01$	$p \leq 0.05$
	LDWW-BD	$p > 0.1$	$p \leq 0.05$
	LDWW-BW	$p > 0.1$	$p > 0.1$
	BD-BW	$p > 0.1$	$p > 0.1$

BD = Both Dry (n=14)

LDWW = Leeward Dry & Windward Wet (n=25)

LWWD = Leeward Wet & Windward Dry (n=16)

BW = Both Wet (n=10)

*Reconstructed storm-track latitude and intensity at 124°W longitude.

^Significance of differences between subsets determined using ANOVA test for All Groups and *t*-tests for individual subsets.

table S2. Reconstructed storm-track latitude and intensity in La Niña and El Niño years based on multiple ENSO proxy reconstructions.

ENSO source	ENSO phase*	Latitude (°N)**	Intensity (m^2 s^{-2})**
Wilson[1]	La Niña	47.8	439.5
	Neutral	47.5	415.8
	El Niño	46.7	398.1
	Significance^	$p \leq 0.1$	$p \leq 0.01$
McGregor[2]	La Niña	48.3	430.9
	Neutral	47.4	415.1
	El Niño	46.5	390.9
	Significance	$p \leq 0.01$	$p \leq 0.01$
Cook[3]	La Niña	48.0	437.3
	Neutral	47.3	419.6
	El Niño	46.2	389.0
	Significance	$p \leq 0.01$	$p \leq 0.01$
Mann[4]	La Niña	48.2	428.8
	Neutral	47.1	423.9
	El Niño	47.3	400.0
	Significance	$p \leq 0.1$	$p \leq 0.01$

*La Niña, neutral, and El Niño defined as < -1 std dev, ≥ -1/2 std dev & ≤ +1/2 std dev, and > +1 std dev, respectively

**Reconstructed storm-track latitude and intensity at 124°W longitude.

^Significance of differences between La Niña and El Niño subsets determined using *t*-tests.

[1]Wilson *et al.* 2010 (*44*), Jan-Dec NINO3.4 lagged 1 yr (see Materials and Methods), corals and ice core, compared 1728-1995

[2]McGregor *et al.* 2010 (*45*), Jul-Jun NINO3.4, multiproxy, compared 1693-1977

[3]Cook *et al.* 2009 (https://www.ncdc.noaa.gov/paleo/study/8704), Dec-Feb NINO3.4, tree rings, compared 1693-1995

[4]Mann *et al.* 2000 (http://www.cricyt.edu.ar/paleo/ei/ei_data/ninocold-recon.dat), Oct-Mar NINO3, multiproxy, compared 1693-1980